Trigger loop dynamics can explain stimulation of intrinsic termination by bacterial RNA polymerase without terminator hairpin contact

Ananya Ray-Soni[a,b], Rachel A. Mooney[a], and Robert Landick[a,c,1]

[a]Department of Biochemistry, University of Wisconsin–Madison, Madison, WI 53706; [b]Department of Neurology, Massachusetts General Hospital, Harvard Medical School, Boston, MA 02129; and [c]Department of Bacteriology, University of Wisconsin–Madison, Madison, WI 53706

Edited by Peter H. von Hippel, University of Oregon, Eugene, OR, and approved September 25, 2017 (received for review April 14, 2017)

In bacteria, intrinsic termination signals cause disassembly of the highly stable elongating transcription complex (EC) over windows of two to three nucleotides after kilobases of RNA synthesis. Intrinsic termination is caused by the formation of a nascent RNA hairpin adjacent to a weak RNA–DNA hybrid within RNA polymerase (RNAP). Although the contributions of RNA and DNA sequences to termination are largely understood, the roles of conformational changes in RNAP are less well described. The polymorphous trigger loop (TL), which folds into the trigger helices to promote nucleotide addition, also is proposed to drive termination by folding into the trigger helices and contacting the terminator hairpin after invasion of the hairpin in the RNAP main cleft [Epshtein V, Cardinale CJ, Ruckenstein AE, Borukhov S, Nudler E (2007) *Mol Cell* 28:991–1001]. To investigate the contribution of the TL to intrinsic termination, we developed a kinetic assay that distinguishes effects of TL alterations on the rate at which ECs terminate from effects of the TL on the nucleotide addition rate that indirectly affect termination efficiency by altering the time window in which termination can occur. We confirmed that the TL stimulates termination rate, but found that stabilizing either the folded or unfolded TL conformation decreased termination rate. We propose that conformational fluctuations of the TL (TL dynamics), not TL-hairpin contact, aid termination by increasing EC conformational diversity and thus access to favorable termination pathways. We also report that the TL and the TL sequence insertion (SI3) increase overall termination efficiency by stimulating pausing, which increases the flux of ECs into the termination pathway.

transcription | RNA polymerase | trigger loop | intrinsic termination | *Escherichia coli*

Transcription termination is an essential process in all organisms that releases the RNA chain and DNA template from transcribing RNA polymerase (RNAP). Termination prevents unwanted gene expression (1), recycles RNAP for new initiation events (2), and prevents genome-destabilizing collisions with the replication machinery (3). In bacteria, intrinsic termination of the elongating transcription complex (EC) can occur without accessory factors in response to a signal in the DNA and newly synthesized RNA. Intrinsic termination occurs over a 2- to 3-nt window of EC destabilization (4) and is caused by the formation of a GC-rich RNA hairpin in the RNA exit channel of RNAP, immediately upstream of a 3′-terminal, ∼8-nt U-rich RNA tract (U-tract; Fig. 1*A*). Precise termination of the highly stable EC requires rapid entry into a termination pathway before continued nucleotide addition moves the EC beyond the region of destabilization (4–6).

A thermodynamic termination model posits that the relative free energy barriers to termination versus elongation determine the fraction of ECs that terminate; thus, termination efficiency (TE) is kinetically determined by competing rates of nucleotide addition and termination (5, 7) (Fig. 1*B*). The EC is stabilized by polar and van der Waals contacts between RNAP and (*i*) the 9- to 10-bp RNA–DNA hybrid formed within an ∼12-bp transcription bubble, (*ii*) the ∼18 bp of DNA in the downstream DNA channel, and (*iii*) the ∼5 nt of unpaired nascent RNA in the RNA exit channel (8–11). The RNA–DNA hybrid also stabilizes the EC (Fig. 1*B*) by offsetting the cost of melting DNA base pairs in the transcription bubble (8, 12–14). These stabilizing interactions must be broken or counterbalanced to disrupt the EC at a terminator (Fig. 1*C*). At termination sites, this destabilization is accomplished by rU–dA base pairs in the U-tract that weaken the hybrid (15), and by the GC-rich terminator hairpin (T_{hp}) that alters RNA contacts to RNAP (16, 17), prevents EC backtracking that would create a more stable hybrid (8), and indirectly disrupts the upstream ∼3 bp of the hybrid via steric features of RNAP (8, 18). Together, these changes make termination kinetically competitive with elongation (19).

Destabilization of the EC at intrinsic terminators occurs in a multistep pathway. First, the U-tract and surrounding sequences cause RNAP to pause (18, 20) (Fig. 1*C*), which creates a kinetic window for T_{hp} nucleation. This "U-tract pause" likely resembles the recently described nonbacktracked, elemental pause (21, 22), since backtracking at a terminator would inhibit T_{hp} formation. The T_{hp} appears to form in two steps: (*i*) formation of a partial T_{hp} that may resemble so-called pause RNA hairpins, which reach only to 2 to 3 nt upstream from the hybrid and increase pause dwell times, and (*ii*) extension of the T_{hp} to complete its stem, which appears to be rate-limiting for termination. T_{hp} extension is thought to melt the upstream ∼3 rU–dA base pairs in the hybrid because the extended T_{hp} stem is sterically incompatible with these base pairs within RNAP (6, 8, 18, 23). This

Significance

RNA polymerase (RNAP), like many cellular processors of information in DNA and RNA, is a complex macromolecular machine whose multiple structural modules and domains undergo poorly understood conformational changes that mediate information processing. We investigated the role of one such mobile module, the polymorphous trigger loop (TL) of RNAP, in intrinsic transcription termination by bacterial RNAP. The TL folds into a helical hairpin to promote RNA synthesis, but also is proposed to aid termination. By separating effects of the TL and of TL variants on termination from effects on RNA synthesis, we established that TL flexibility, not the helical hairpin conformation, facilitates rearrangements of RNAP leading to termination. Our results illustrate how kinetic assays can help dissect complex macromolecular machines.

Author contributions: A.R.S. and R.L. designed research; A.R.S. performed research; A.R.S. and R.A.M. contributed new reagents/analytic tools; A.R.S. and R.L. analyzed data; and A.R.S. and R.L. wrote the paper.

The authors declare no conflict of interest.

This article is a PNAS Direct Submission.

[1]To whom correspondence should be addressed. Email: landick@bact.wisc.edu.

This article contains supporting information online at www.pnas.org/lookup/suppl/doi:10.1073/pnas.1706247114/-/DCSupplemental.

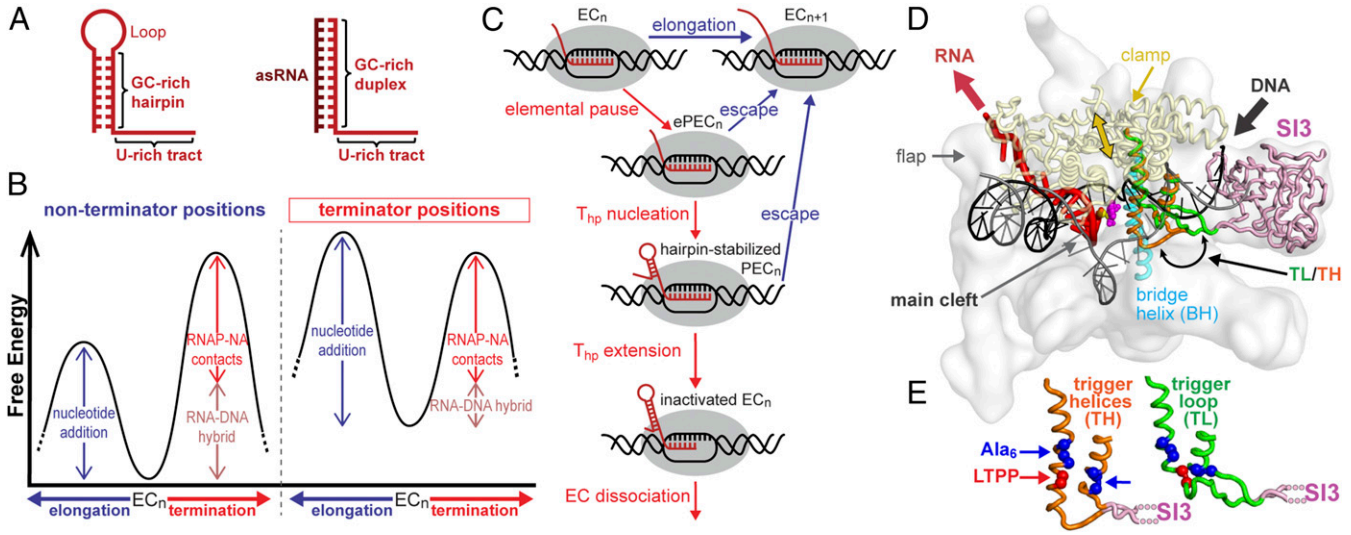

Fig. 1. Intrinsic transcription termination and the polymorphous TL. (*A*) (*Left*) The main elements of a canonical intrinsic terminator are shown: a U-rich tract, immediately preceded by a GC-rich T_{hp} structure. (*Right*) The T_{hp} can be mimicked by annealing an asRNA (antisense RNA; dark red) complementary to the nascent RNA transcript (light red) to create a GC-rich duplex. (*B*) The thermodynamic model for termination (4–6), in which the relative free energy barriers to elongation (blue) versus termination (red) determine the probability of each event. The stabilities of the RNA–DNA hybrid (pink) and RNAP–NA interactions (red) are proportional to the arrow height. (*C*) The steps of intrinsic termination. Steps that lead to termination are indicated by red arrows; steps that lead to terminator bypass are indicated by blue arrows. RNA, red; DNA, black; RNAP, gray. (*D*) Structure of an EC and relevant elements generated as described in ref. 37. RNAP is shown as a white surface with modules of interest shown as Cα backbone traces. The alternative structures of the folded TH (orange) and the unfolded TL (green) structures are both shown. For clarity, the TL insertion (SI3, pink) is shown connected to the unfolded TL conformation. (*E*) The TH and unfolded TL conformations. Blue and red spheres indicate residues mutated in the folded TL stabilizing (Ala_6) and folded TL destabilizing (LTPP) RNAP mutants, respectively.

hybrid melting may occur in alternative pathways, depending on hybrid sequence (24, 25): (*i*) In hybrid-shearing, the extending T_{hp} pulls the RNA out of register from the DNA by shearing a perfect or near-perfect rU–dA hybrid (8, 24), or (*ii*) in hyper-translocation when shearing is unfavorable, T_{hp} extension pulls the entire hybrid upstream by melting upstream RNA–DNA base pairs and downstream DNA duplex base pairs without complementary ribonucleotide addition (24–26). By either route, the remaining partial hybrid cannot stabilize the EC sufficiently and EC dissociation becomes favorable (8).

In contrast to the role of nucleic acid (NA) base pairing, the contributions of structural changes in RNAP modules and domains to termination remain incompletely described (25, 27). A complexity of multiple moving domains and refolding modules is a common feature of macromolecular machines that process information in RNA and DNA. In RNAP, a hinged clamp domain forms stabilizing contacts to both RNA and DNA and may need to open for EC dissociation (17, 28–31). In addition, a highly conserved, polymorphous, ∼47-aa trigger loop (TL; Fig. 1 *D* and *E*) (32–34) undergoes random coil to helical hairpin transitions during catalysis of nucleotide addition (32, 34). At intrinsic terminators, the T_{hp} is proposed to invade the RNAP main cleft and to stimulate termination via a direct contact to the TL in its helical hairpin conformation, also called the trigger helices (TH) (28). A TH–T_{hp} contact has yet to be observed in EC structures, and this TH–T_{hp} contact model of termination has been disputed (35). Thus, understanding the role of the TL in termination provides a useful case study for understanding roles of dynamic modules in macromolecular machines generally.

To investigate the role of the TL in termination, we developed an experimental approach that can separate effects on termination rate from effects on elongation rate, which are known to be significant for TL alterations (36–38). Whereas traditional TE measurements report an aggregate of effects on termination and elongation, isolated measurement of termination rate in our assay allowed us to determine the effects of TL mutations specifically on the termination mechanism. Using RNAP variants that (*i*) bias the TL toward either the folded or unfolded states, (*ii*) remove the sequence insertion 3 (SI3) from the TL, or (*iii*) delete the polymorphous arms of the TL, we were able to test the contribution of the TL to termination rate, TE, and the pausing steps leading into the termination pathway.

Results

Measurement of Termination by Elongation-Compromised RNAP Mutants. To investigate the effect of the TL on intrinsic termination, we needed to separate effects of EC rearrangements on the termination pathway, in which TH–T_{hp} contact is proposed to play a role, from effects on the rate of nucleotide addition, which affects TE by competing with the termination pathway and is known to depend on TL folding.

We first investigated a strategy to study termination by measuring dissociation rates of static ECs stalled by NTP deprivation. We triggered formation of a T_{hp} mimic by addition of antisense oligonucleotides (oligos) to the static ECs to stimulate termination (8, 18). However, we found that stalled ECs terminated more slowly than active ECs and were largely insensitive to TL alterations, contrary to demonstrated TL effects on termination (28) (*SI Appendix, Supplementary Discussion* and Fig. S1). This result may reflect the fact that stalled ECs can isomerize into alternative conformations before termination is triggered by addition of the antisense oligo. To avoid artifactual effects in static ECs, we instead developed an active EC termination assay in which termination was triggered in actively elongating ECs by antisense oligo addition.

To develop the active-EC termination assay, we modified the hairpin-stabilized *his* pause sequence to resemble an intrinsic terminator by adding rU–dA base pairs to create a terminator U-tract (t_{his2}; Fig. 2*A*). We also removed the upstream arm of the pause hairpin, which allowed assembly of stable ECs at G17 and measurement of rates of elongation and pausing at C18 and U19 in the absence of a complete termination signal. Antisense oligos that pair to the exiting RNA 8 nt to 10 nt from the U19 RNA 3′ end could then be added to create a T_{hp} mimic (20) for measurement of the termination rate at U19, corresponding to

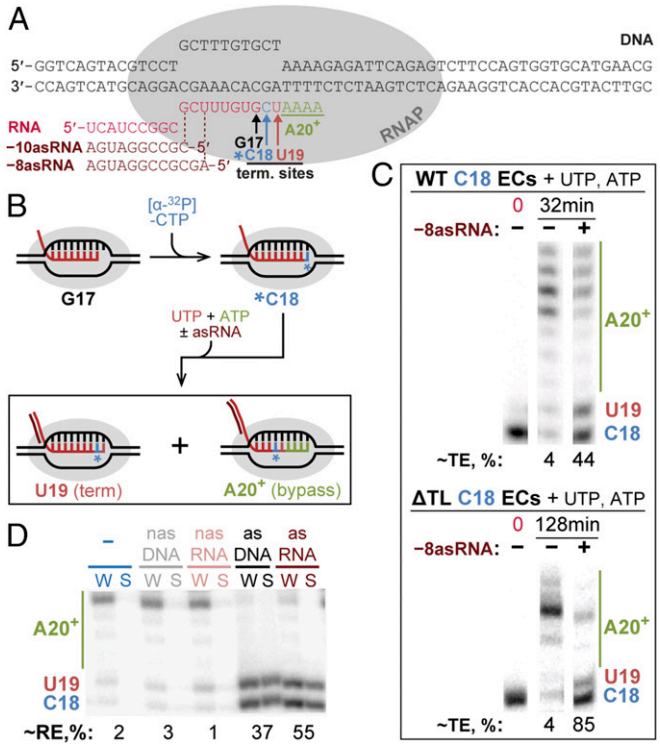

Fig. 2. Measuring termination by elongation-compromised RNAP mutants. (*A*) The t_{his2} terminator sequence and asRNAs are shown. The −8 asRNA and −10 asRNA pair at their 5′ ends to the −8 and −10 RNA bases, respectively (where the 3′ nt of U19 RNA is −1). The asterisk denotes the radiolabel at C18 in the nascent RNA. Termination is observed at two sites on t_{his2}, C18 and U19. (*B*) Key steps in the t_{his2} termination assay. ECs are reconstituted at G17, radiolabeled at C18, and extended past U19 in the presence or absence of asRNA. (*C*) WT and ΔTL ECs elongate past the termination sites in the absence of asRNA, but terminate efficiently in its presence. WT and ΔTL C18 ECs were assembled as depicted in *B*. WT ECs were extended with 100 μM UTP and 10 μM ATP for 32 min in the presence or absence of 50 μM −8 asRNA. ΔTL C18 ECs were extended with 10 mM UTP and ATP, and 50 μM −8 asRNA added after 280 s to allow initial U19 accumulation. ΔTL reactions were incubated for 128 min to ensure completion. For WT ECs, TE was calculated as the percent of U19 ECs that terminated, i.e., TE = U19/(U19 + A20$^+$) × 100. To account for delayed asRNA addition for ΔTL ECs, TE for ΔTL ECs was calculated as the percent of U19 RNA present at the time of asRNA addition that failed to extend to A20$^+$. (*D*) Robust termination and release of C18 and U19 RNAs occurs with oligos complementary to the exiting RNA (asDNA/asRNA), but not with noncomplementary oligos (nasDNA/nasRNA). G17 ECs were tethered to paramagnetic Co^{2+} beads via a His_{10} tag on RNAP. The RNAs were radiolabeled at C18 and then extended through U19 with 100 μM UTP and 10 μM ATP in the absence or presence of 50 μM antisense or noncomplementary control oligo. The asRNA is equivalent to −8 asRNA in *A*. Release efficiency (RE) was calculated as the amount of C18 and U19 RNA that is released in the supernatant (S) as a fraction of total RNA present in the whole reaction (W). W = pellet (RNAP-bound RNA) + S (released RNA).

the typical position of intrinsic termination. Because ECs are known to reset to a naïve conformational state after each round of nucleotide addition (39), comparison of termination rates only at U19 after restarting transcription from halted C18 ECs further ensured that the measured rates were derived from active complexes (Fig. 2*B*). By using high concentrations of antisense oligos, we ensured that the T_{hp} duplex nucleated quickly in all ECs. With appropriate assay conditions (*Methods*, Fig. 3, and *SI Appendix*, Figs. S7, S8, and S10), both elongation and termination occurred within measureable time ranges. This assay design prevented three distinct problems observed on other sequences we tested: (*i*) spontaneous EC dissociation due to an unstable RNA–DNA hybrid, (*ii*) backtracking of ECs and intrinsic cleavage of the nascent RNA before addition of the antisense oligo, and (*iii*) inefficient or slow termination.

Using this design, we first tested transcription of t_{his2} by wild-type (WT) and TL-deletion (ΔTL) (*SI Appendix*, Table S1) RNAPs in the absence of the T_{hp} (Fig. 2*A*). ECs were reconstituted at G17, radiolabeled by incorporation of [α-^{32}P]CMP, and then elongated through U19 by incubation with UTP and ATP (Fig. 2 *B* and *C*). Although ΔTL ECs required high (10 mM) UTP and ATP concentrations, we observed near-complete elongation past the termination site for both WT and ΔTL ECs. We next examined the effect of complementary (antisense) and control noncomplementary DNA and RNA oligos added with the UTP and ATP on transcription of t_{his2} by WT RNAP. RNAP was immobilized on Co^{2+} beads via a His_{10} tag to enable the detection of RNA release. As observed previously (20, 26, 40, 41), only the complementary oligos stopped RNAP at C18 and U19 (Fig. 2*D*) and caused release of the C18 and U19 RNAs into the supernatant, verifying that they were terminated. Because antisense RNA (asRNA) stimulated more termination than antisense DNA (asDNA) and generates a duplex similar to a natural T_{hp}, we used asRNAs for all subsequent experiments.

For our measurements, we focused on the U19 position where all ECs were actively elongating. We used two asRNAs that either disrupted the upstream-most hybrid base pairs and gave higher TE (−8 asRNA) or destabilized hybrid base pairs only indirectly and gave lower TE (−10 asRNA) (Fig. 2*A*). Because reliable calculation of termination rate in our assay required a TE between 15% and 85% and because some RNAPs gave TEs outside this range, only the −8 or −10 asRNA worked well for some RNAP variants.

Deletion of the TL Increases TE. We first tested whether deletion of the TL would affect termination, as predicted (28). Radiolabeled WT and ΔTL C18 ECs were assembled as described in *Measurement of Termination by Elongation-Compromised RNAP Mutants*, and then elongated through U19 with UTP and ATP in the presence of −8 asRNA (Fig. 2 *A*–*C*). The addition of asRNA to ΔTL (but not WT) ECs was delayed to allow U19 ECs to accumulate. The TE at U19 was greater for ΔTL ECs (~85%) than for WT ECs (~44%), even at the high NTP concentrations used for ΔTL ECs (Fig. 2*C* and Table 1). Thus, our results verified that the TL affects TE. However, to test the TH–T_{hp} contact model (28) unambiguously, we needed to measure the effect of the TL on termination rate (rather than the composite TE); the model predicts termination rate will be slowed when the TH–T_{hp} contact is removed. Therefore, we next sought to measure elongation rate and termination rate at t_{his2} separately.

The TL Strongly Stimulates the Rate of Intrinsic Termination. To separate elongation and termination rates, we next measured transcription of t_{his2} by WT and ΔTL ECs using time-resolved assays, which required use of a quench-flow apparatus for WT ECs (*Methods*). By first omitting asRNA, we could obtain elongation rates and pause rates, which were then used as constants to derive termination rates from best-fit numerical integration of kinetic models of transcription in the presence of asRNA.

Radiolabeled C18 WT and ΔTL ECs were assembled and elongated through U19 with or without asRNA as described in *Deletion of the TL Increases TE*, except that samples were removed and quenched at time points during the reactions (Fig. 3 *A*–*C* and *SI Appendix*, Fig. S2 *A* and *B*). The WT and ΔTL EC elongation and pause rates were determined by fitting the proportion of C18, U19, and ≥A20 (A20$^+$) complexes present at each time point in the absence of asRNA to kinetic models that included C18-to-U19, U19-to-A20, and elemental pausing steps at C18 or U19 as necessary by numerical integration using Kintek Explorer (42) (*Methods*, Fig. 4, and *SI Appendix*, Fig. S3). We tested kinetic models for least-squares fit to the observed data using the corrected Akaike's Information Criterion (43), and the

Table 1. Effects of TL mutations on the termination rate and efficiency at U19

RNAP	asRNA	TE*	k_{term}, $\times 10^{-4}$ s^{-1}	k_{term} ratio†
WT	−8	42 ± 3	1,000 ± 300	N.D.
	−10	17 ± 1	260 ± 20	4 ± 1‡
ΔTL	−8	87 ± 7	N.D.	N.D.
	−10	26 ± 2	3.5 ± 0.2	74 ± 7
ΔSI3	−8	34 ± 7	850 ± 150	1.2 ± 0.4
	−10	~4§	N.D.	N.D.
LTPP	−8	86 ± 1	N.D.	N.D.
	−10	47 ± 7	6.6 ± 0.5	39 ± 4
LTPPΔSI3	−8	99 ± 2	N.D.	N.D.
	−10	53 ± 2	14 ± 2	19 ± 3
Ala_6ΔSI3	−8	~86§	N.D.	N.D.
	−10	44 ± 9	14 ± 3	19 ± 4

N.D., not determined because the TE was outside the useful range of the assay (15–85% TE). Errors are SD of values calculated from ≥3 independent experimental replicates.

*TE = U19/(U19 + $A20^+$) × 100, where $A20^+$ includes RNA products A20 or larger; TE calculations were adjusted for conditions with delayed asRNA addition by determining the percent of U19 RNA present at the time of asRNA addition that failed to extend to $A20^+$.

†Here k_{term} ratio = k_{term}(WT)/k_{term}(mutant) for a given asRNA.

‡Here k_{term} ratio = k_{term}(WT with −8 asRNA)/k_{term}(WT with −10 asRNA).

§Value reported is the average of two replicates.

simplest kinetic model with statistically significant improvement relative to alternatives was chosen (*Methods* and *SI Appendix*, Fig. S3). A significant fraction of WT ECs paused at C18 and U19 in response to the U-tract sequence (Fig. 4 and Table 2). However, ΔTL ECs elongated through C18 and U19 with simple pseudo first-order kinetics, consistent with the previous finding that ΔTL ECs do not exhibit pausing behavior (22).

Initially we compared WT and ΔTL RNAPs using the −8 asRNA (*SI Appendix*, Fig. S4 *A–D*), but found that the TE for ΔTL RNAP was too high to allow reliable calculation of the termination rate (Table 1). Shifting the asRNA to extend only to −9 (relative to U19 at −1) also gave near 100% TE for ΔTL RNAP (*SI Appendix*, Fig. S4 *E* and *F*). Therefore, we chose the −10 asRNA to enable accurate comparison of termination rates of WT and ΔTL RNAPs.

The rates of termination were calculated by fitting the relative populations of C18, U19, and $A20^+$ RNA species observed in the presence of −10 asRNA (Fig. 3 *D* and *E* and *SI Appendix*, Fig. S2 *C* and *D*) using the best-fit kinetic model of elongation and pausing with fixed rates of elongation, pause entry, and pause escape, and unconstrained rates of termination for positions C18 and U19 (Fig. 5). In addition, inclusion of a fixed rate of asRNA pairing, which was measured separately using a previously described assay (44) (*SI Appendix*, Fig. S5), and of unconstrained rates of nucleotide addition for the RNA duplex-containing EC states were required to give good fits to the data (*Methods* and *SI Appendix*, Fig. S6). Thus, in our calculations of termination rates, only four parameters were allowed to vary: the rates of elongation and termination by −10 asRNA-bound C18 and U19 ECs (black arrows in Fig. 5).

To avoid potential artifacts from comparing the behaviors of halted C18 ECs (*SI Appendix, Supplementary Discussion*), we compared WT and ΔTL termination rates for U19 ECs (k_{term}; Fig. 5). Despite the increased TE observed for ΔTL ECs (Fig. 2*C* and Table 1), k_{term} was decreased by a factor of ~75 in ECs lacking a TL ($[3.5 \pm 0.2] \times 10^{-4}$ s^{-1} for ΔTL vs. $[260 \pm 20] \times 10^{-4}$ s^{-1} for WT; Table 1). Although deleting the TL slows termination rate dramatically, overall TE changes much less (Table 1) because the TL deletion also decreases nucleotide addition rate (Fig. 4 and Table 2). This masking of a large effect on termination rate when considering only the aggregate TE illustrates

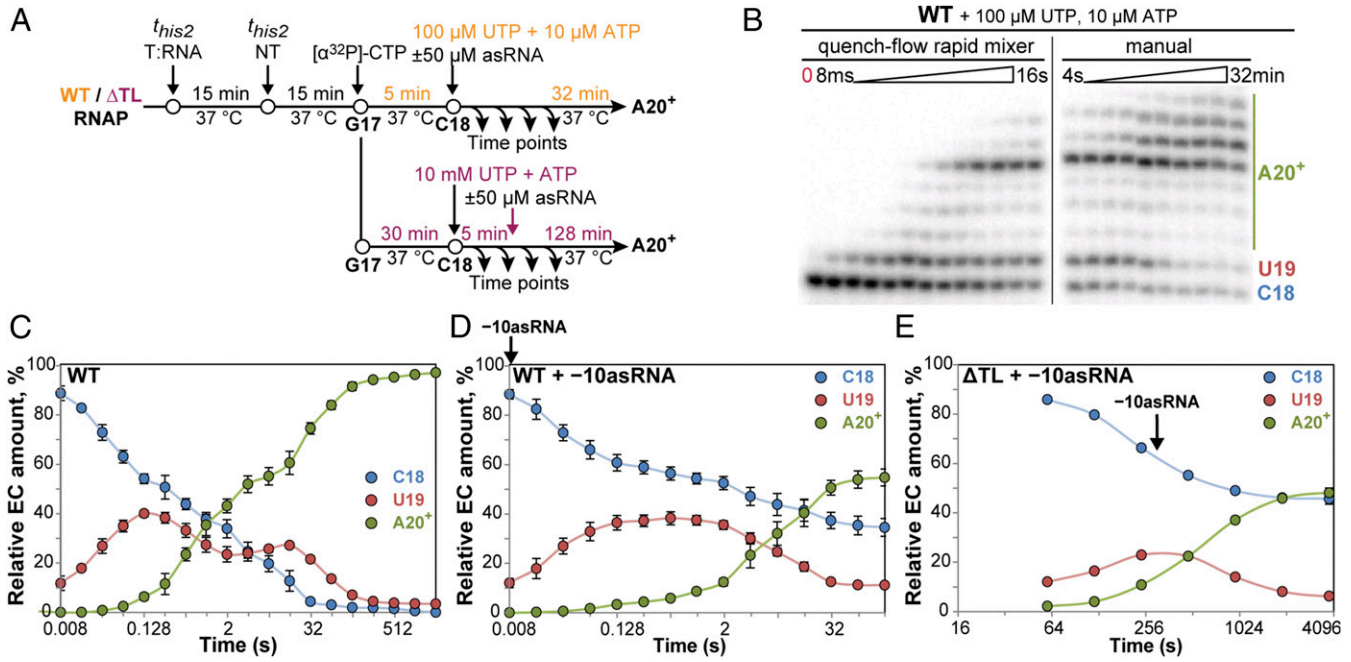

Fig. 3. Limited hairpin extension enabled termination rate measurements for slow ΔTL RNAP mutant. (*A*) Experimental scheme for measurement of the elongation and termination rates of WT and ΔTL ECs. (*B*) Representative denaturing RNA gel image and (*C*) reaction progress curves showing the conversion of RNAs from C18 to U19 to $A20^+$ for WT ECs in the absence of asRNA. The ΔTL gel image and reaction progress curves are shown in *SI Appendix*, Fig. S2 *A* and *B*. (*D* and *E*) Reaction progress curves for (*D*) WT ECs with −10 asRNA and (*E*) ΔTL ECs with −10 asRNA; the corresponding gel images are shown in *SI Appendix*, Fig. S2 *C* and *D*, respectively. The time of asRNA addition is indicated with arrows. Error bars represent SD from three or more independent experimental replicates; error bars are smaller than the data markers in some cases.

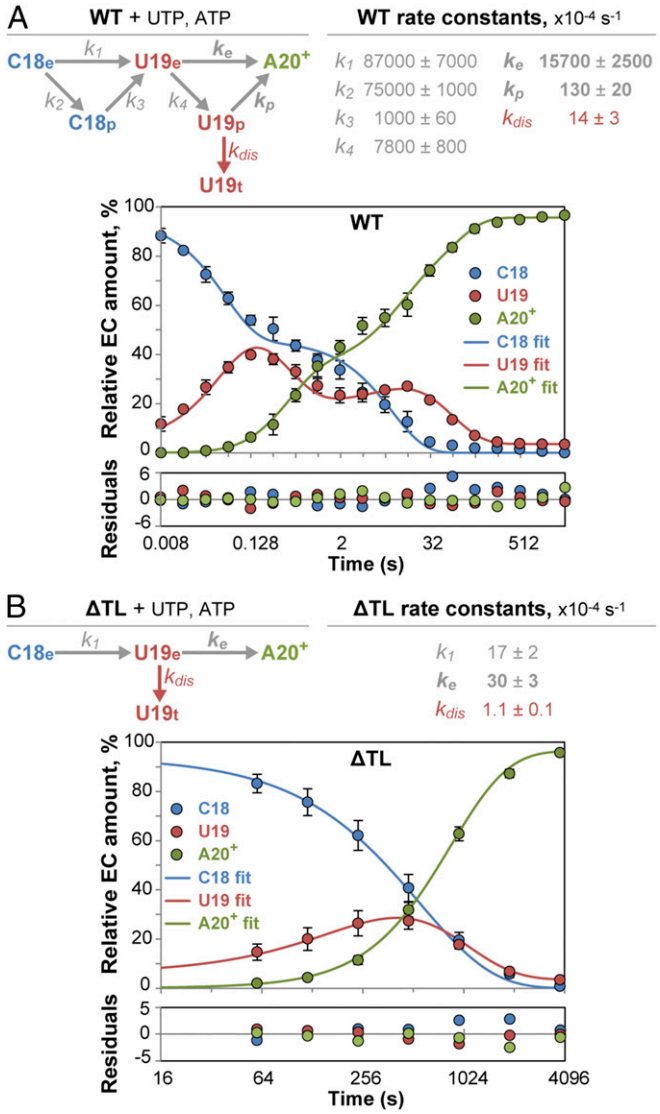

Fig. 4. Determination of elongation rates in the absence of asRNA by kinetic fitting. Kinetic models, the corresponding fits, and the rate constants obtained from the fits are shown for (*A*) WT and (*B*) ΔTL ECs in the absence of asRNA. Residuals between measured EC amounts and the amounts predicted by the kinetic mechanisms and rate constants from global fits are shown in the lower panels. $C18_e$, $U19_e$, and $A20^+$ denote elongating ECs with C18, U19, or $A20^+$ RNAs, respectively; $C18_p$ and $U19_p$, elemental paused ECs; $U19_t$, terminated ECs. Error bars represent SD from three or more independent experimental replicates (*Methods*); error bars are smaller than the symbols in some cases.

the importance of measuring the termination rate to study the mechanism of termination. We conclude that the TL plays a crucial role in intrinsic termination by significantly accelerating the rate-limiting step in the termination pathway.

We note that −8 asRNA accelerated termination rate ~fourfold relative to −10 asRNA ($[1{,}000 \pm 300] \times 10^{-4}$ s^{-1} for −8 asRNA vs. $[260 \pm 20] \times 10^{-4}$ s^{-1} for −10 asRNA; Table 1), consistent with the idea that T_{hp} extension is at least partially rate-determining for EC inactivation.

The TL also Aids Termination by Favoring Pausing at the Termination Sites. Our kinetic analyses also yielded estimates for the rates of pause entry and escape for WT and ΔTL ECs. One-third (33%) of WT U19 ECs entered a paused state in which nucleotide addition was slowed by a factor of ~120 in the absence of asRNA, or by a factor of ~16 after asRNA binding (Fig. 4*A* and Table 2). However, the absence of the TL completely abrogated pausing at U19 in response to the U-tract (Fig. 4*B* and Table 2). The presence of the TL thus favors entry into the elemental paused state in WT ECs, which would extend the kinetic window for T_{hp} formation. The binding of asRNA also had minimal effect on nucleotide addition rate by ΔTL RNAP (Table 2), consistent with previous reports that the TL participates in the hairpin-stabilized paused state (22, 37, 45). We conclude that, in addition to stimulating termination, the TL helps establish and inhibits escape from paused states at terminators, thereby increasing flux of ECs into the termination pathway.

SI3 Increases Pausing and TE, but Not Termination Rate. The *Escherichia coli* TL contains a large (188-aa) insertion called SI3 (Fig. 1 *D* and *E*), present in many Gram-negative bacterial lineages (46, 47). SI3 affects TL function in elongation, pausing, and intrinsic cleavage (37, 48, 49). A monoclonal antibody (mAb) that binds SI3 was shown to decrease dissociation of ECs stalled at a termination site (28). Thus, the effect of TL deletion on termination observed in our assay could reflect effects of the TL itself or of SI3, which is also deleted in ΔTL RNAP.

To test for SI3 effects on termination, we determined elongation, pause, and termination rates of an SI3 deletion mutant (ΔSI3; *SI Appendix*, Table S1) on the t_{his2} scaffold. Termination was almost undetectable for ΔSI3 ECs with −10 asRNA, suggesting that SI3 either aids termination rate or increases the formation or dwell time of paused states leading to termination. The −8 asRNA caused ~35% TE for ΔSI3 RNAP and enabled direct comparison of termination rate to WT (Table 1 and *SI Appendix*, Fig. S7). Interestingly, deletion of SI3 had little effect on termination rate (Table 1). Therefore, the strong effect of the TL deletion on termination rate reflects a role of the TH-forming parts of the TL and not an effect of SI3 on termination rate.

Although SI3 did not affect termination rate, it did increase pausing significantly, with the indirect effect of increasing TE by increasing flux of ECs into the termination pathway. Deletion of SI3 decreased relative pause lifetime at U19 by a factor of ~15 ([8 ± 3] for ΔSI3 vs. [120 ± 30] for WT; Table 2), and decreased the fraction of U19 ECs that entered the paused states (~17% for ΔSI3 vs. ~33% for WT). However, SI3 had less effect on the rate of A20 addition after asRNA binding (Table 2). Although an approximately threefold effect of SI3 on pausing stabilized by a hairpin extending to −12 has been observed previously (37, 49), the closer approach of the duplex stem to the RNA 3′ end may obviate this effect of SI3 at terminators (50). As a consequence of less pausing overall, the TE for ΔSI3 ECs was ~34% vs. ~42% for WT (Table 1), indicating that SI3-mediated pause stimulation increased TE by increasing flux of ECs into the termination pathway, even though the termination rate per se was minimally affected.

Reduced TL Conformational Flexibility Inhibits Termination Rate. Our results established that the TL increases termination rate up to ~75-fold. However, it was unclear if a particular TL state (e.g., the TH as predicted by the TH–T_{hp} contact model) favors termination, if some other conformation favors termination, or if the conformational flexibility of the TL might be more important than any single conformation. To address these questions, we sought to test termination at t_{his2} by previously characterized TL variants that either stabilize the folded TL conformation (Ala_6) or prevent folding and favor unfolded conformations (LTPP; Fig. 1*E*) (36, 37). For the TH-destabilizing LTPP substitution, we could make a direct comparison between the mutant RNAP and WT using the −10 asRNA (*SI Appendix*, Fig. S8). The LTPP substitutions decreased termination rate by a factor of ~40, similar to the effect seen for ΔTL using the −10 asRNA (Table 1).

Table 2. Effects of TL mutations on pausing on the termination pathway at U19

RNAP	asRNA	[ATP]	k_e, $\times 10^{-4}$ s^{-1}	PE*	k_p, $\times 10^{-4}$ s^{-1}	k_e/k_p	$k_{p,asR}$, $\times 10^{-4}$ s^{-1}	$k_e/k_{p,asR}$
WT	−8	10 μM	15,700 ± 2,500	33 ± 2	130 ± 20	120 ± 30	980 ± 400	16 ± 7
	−10	10 μM					980 ± 100	16 ± 3
ΔTL	−10	10 mM	30 ± 3	N.A.	N.A.	N.A.	20.3 ± 0.2	1.5 ± 0.2
ΔSI3	−8	10 μM	14,200 ± 1,000	17 ± 2	1,800 ± 600	8 ± 3	1,080 ± 300	13 ± 4
LTPP	−10	10 mM	42 ± 1	N.A.	N.A.	N.A.	13.4 ± 0.3	3.1 ± 0.1
LTPPΔSI3	−10	10 mM	62 ± 2	N.A.	N.A.	N.A.	21 ± 3	3 ± 0.4
Ala_6ΔSI3	−10	10 μM	83 ± 4	N.A.	N.A.	N.A.	19 ± 3	4.4 ± 0.7

Errors are SD of values calculated from three or more independent experimental replicates. N.A., not applicable.
*PE (pause efficiency), percent of complexes that enter the U-tract paused state, $U19_p$.

Unfortunately, we were unable to make a direct comparison between WT and the TH-stabilizing Ala_6 RNAP because C18 ECs formed with Ala_6 RNAP exhibited spontaneous transcript cleavage that precluded subsequent analyses (*SI Appendix*, Fig. S9*A*). However, we could make an indirect comparison using Ala_6ΔSI3 RNAP with −10 asRNA (*SI Appendix*, Fig. S10), even though −10 asRNA TE for ΔSI3 RNAP was too low for kinetic modeling and −8 asRNA TE for Ala_6ΔSI3 RNAP was too high for kinetic modeling (*SI Appendix*, Fig. S9 *B* and *C*). The −10 asRNA termination rate for Ala_6ΔSI3 RNAP was slower by a factor of ∼20 compared with WT RNAP. Since we found that SI3 itself had little effect on termination rate (Table 1), this indirect comparison suggests that the TH-stabilizing Ala_6 substitutions are responsible for the large effect on termination rate. Consistent with this interpretation, the −10 asRNA termination rate for LTPPΔSI3 RNAP was slower by a factor of ∼20 compared with WT RNAP and similar to the ∼40-fold effect of LTPP on termination rate observed when SI3 was present (Table 1 and *SI Appendix*, Fig. S10). We conclude that both the TH-destabilizing LTPP substitutions and the TH-stabilizing Ala_6 substitutions cause large decreases in termination rate on the t_{his2} scaffold.

The Ala_6 and LTPP results together indicate that neither the folded nor unfolded TL per se aids termination. However, both Ala_6 and LTPP TLs gave faster termination rates than the TL deletion (Table 1). These results suggest that restricting TL movements into a smaller conformational space may reduce termination by lessening the probability that the flexible RNAP structure can access termination pathways with lower barriers to termination (*Discussion*).

Discussion

Our study revealed effects of TL conformational states on the rate of intrinsic termination by exploiting an assay that derives termination rates from measurements of elongation rates, pause rates, and TE. This approach was necessary to study the effects of the TL on termination because TL alterations can profoundly impact elongation rates and pause propensities of ECs, and thus can greatly affect TE irrespective of effects on termination rate. Using this assay, we were able to isolate individual steps in the kinetically complex termination pathway and gain several insights into the role of the TL at key decision points along the termination pathway (Fig. 6). First, the TL enhanced the rate of termination, independent of its effects on pausing and elongation. Second, the polymorphous arms of the TL, not the 188-aa TL insertion (SI3), were responsible for the effect on termination rate. Third, both the TL and SI3 increased the flux of ECs into the termination pathway by promoting pausing. Finally, in contradiction to the TH–T_{hp} contact model (28), our results suggest that conformational fluctuations of the TL—i.e., its ability to adopt different conformations and not the TH conformation required for contact to the T_{hp}—accelerate the rate-limiting step of intrinsic termination.

A Model for Termination Aided by TL Conformational Dynamics. The thermodynamic model of intrinsic termination posits that the relative free energy barriers to elongation and termination determine the fraction of complexes that terminate via kinetic competition between the two pathways (4, 5) (Fig. 1*B*). This model, with single elongation and termination pathways and simple changes to RNAP–NA contacts, was sufficient before knowledge that modules like the clamp, bridge helix, and TL occupy distinct, interconnected conformational states (17, 29–31, 44, 51, 52). Incorporation of these states and the known alternatives of hybrid shearing or hypertranslocation (24) suggests an extension of the thermodynamic model to a multistate multipath (MS-MP) model, in which different interconverting EC conformations explore multiple, alternative termination pathways (Fig. 6).

The MS-MP termination model posits that the terminating EC exists in a family of conformational states with fluctuating RNAP–NA contacts that are weaker in some states than in others. These conformational fluctuations would result in variations in EC stability (Fig. 6*B*, *Inset*) and create multiple paths to termination with different free energy barriers (Fig. 6*B*). Variability in free energy barriers caused by multiple molecular states has precedent in studies of ligand binding and catalysis, where differences between protein conformational substates and their relative stabilities are thought to cause variations in the activation energy of different pathways (53–58). The idea of multiple parallel routes for a single reaction is analogous to the well-documented concept of multiple protein folding pathways (55, 56, 59). The hybrid-shearing and hypertranslocation termination models (8, 24, 26) are examples of such different pathways in the case of intrinsic termination. The MS-MP model is similar to the original thermodynamic termination model developed by von Hippel and coworkers (4–6), but adds the dimension of protein conformational states that were not well defined when the model was developed.

A principal rationale for the MS-MP termination model is in its ability to provide a parsimonious explanation for both the ∼75-fold stimulatory effect of the TL on termination rate and the reduction in termination rate when either the folded or unfolded TL conformation is stabilized (Table 1). If terminating ECs occupy multiple states with multiple possible paths to termination as proposed by the MS-MP model, conformational changes in the mobile TL that increase the conformational diversity of terminating ECs would enable the ECs to access pathways with lower free energy barriers to termination (Fig. 6*B*). The MS-MP model thus predicts that, when the TL is deleted or its conformations restricted by alterations (as in Ala_6 and LTPP RNAPs), the number of accessible conformational states of the terminating EC will be reduced (*SI Appendix*, Fig. S11, *Inset*). Restricting conformational states will inhibit access to lower-energy paths of termination (*SI Appendix*, Fig. S11, highlighted areas) and decrease overall termination rate, consistent with the effects of TL alterations reported here (Table 1). Conversely, a dynamic TL

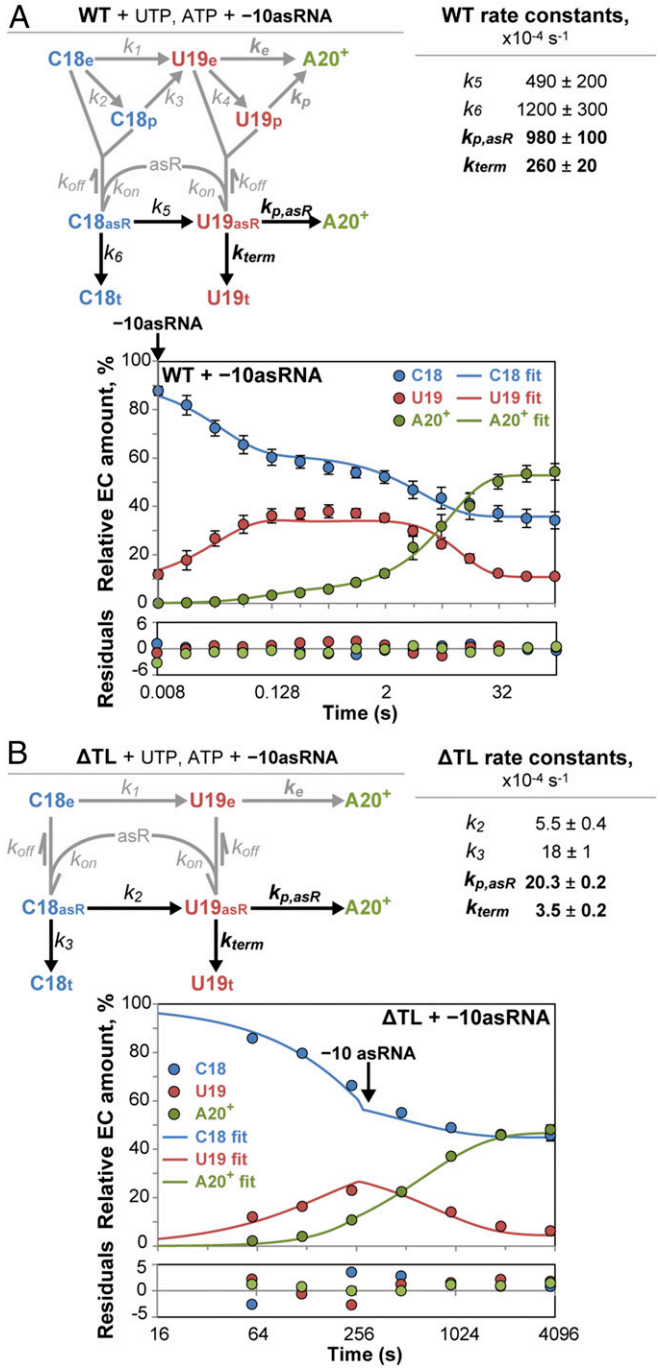

Fig. 5. The TL increases termination rate. Kinetic models, the corresponding fits, and the rate constants obtained from the fits are shown for (*A*) WT and (*B*) ΔTL ECs with −10 asRNA. Time of asRNA addition is indicated with arrows, and is accounted for in the kinetic fits. Residuals between measured EC amounts and the amounts predicted by the kinetic mechanisms and rate constants from global fits are shown in the lower panels. $C18_e$ and $U19_e$ denote elongating ECs with C18 or U19 RNAs, respectively; $C18_p$ and $U19_p$, elemental paused ECs; asR, free asRNA; $C18_{asR}$ and $U19_{asR}$, asRNA-bound ECs; $C18_t$ and $U19_t$, terminated ECs; $A20^+$, ECs with $A20^+$ RNA. Error bars represent SD from three or more independent experimental replicates (*Methods*); error bars are smaller than the symbols in some cases.

that fluctuates among various conformations will enable the EC to explore multiple routes of termination and increase the overall termination rate. In this view, the observed termination rates are aggregates of multiple termination paths, and lessening the conformational flexibility of RNAP reduces the probability of termination.

Inhibition of Termination by TH Stabilization Contradicts the TH–T_{hp} Contact Model. The TH–T_{hp} contact model posits that formation of the TH favors termination by contacting the T_{hp} (28). However, stabilization of the TH by Ala substitutions in the TL/TH hinge regions inhibited termination (Table 1, Ala_6ΔSI3). This result, coupled with alternative explanations for the main findings based on which the TH–T_{hp} contact model was proposed (35), favor the MS-MP termination model.

The TH–T_{hp} contact model is based, in part, on the observation of UV-induced crosslinks between the upper stem and loop of the T_{hp} and the TL, leading to the suggestion that the T_{hp} invades the main cleft of RNAP and contacts the TH in a terminating complex (18, 28). However, the low-salt conditions in which this crosslink can be detected cause the formation of binary RNA–RNAP complexes after EC dissociation (60); these posttermination binary complexes are the likely source of the crosslink (35). Moreover, a TL substitution found to inhibit termination (G1136S) (28) likely favors the TH conformation (51), whereas binding of a mAb to SI3 that stabilizes an unfolded TL also inhibits termination (28). The similar inhibitory effects of biasing the TL in opposing orientations are at odds with the TH–T_{hp} contact model but consistent with the MS-MP model. Finally, based on inhibition of termination by the TH-stabilizing ligand tagetitoxin, it also has been argued that the unfolded TL rather than the folded TH favors Rho-dependent termination (61). It is improbable that Rho-dependent and Rho-independent (intrinsic) termination would be favored by opposite TL conformations, putting the TH–T_{hp} contact model at odds with the proposed role of the TL in Rho-dependent termination. However, these effects are all readily explained by the MS-MP model, where different means of restricting TL conformational fluctuations all result in decreased termination rate.

The TL and SI3 also Promote Intrinsic Termination by Stimulating Transcriptional Pausing. Prior studies suggest that pausing plays a key role in termination, by allowing time for the T_{hp} to form and then to invade and destabilize the EC (18, 20, 23, 50, 62). Pausing is thought to be mediated, in part, by inhibition of TL folding aided by SI3 (22, 37, 45). Our results confirm these hypotheses and provide quantification of the effects of pausing and of the TL during termination at an active terminator, whereas earlier studies inferred roles of pausing from studies in which the T_{hp} was unable to form completely.

For WT RNAP, we could resolve two distinct paused states at U19. One paused state existed before (or in the absence of) asRNA binding with a nominal dwell time ~100 times slower than the elongation pathway (Table 2). This pause was consistent with prior descriptions of pausing in the terminator U-tract and with the properties of an elemental pause (18, 20–22). A distinct paused state existed after asRNA binding, in which the paused ECs were still capable of escape by nucleotide addition but at a rate ~20 times slower than the elongation pathway. The shorter lifetime of the RNA duplex-containing paused ECs (relative to the pause observed when the duplex was absent) is consistent with prior studies suggesting that extension of an exit channel duplex to 11 nt or less from the RNA 3′ end eliminates most of the pause-prolonging effects of exit-channel duplexes that extend to −12 or −13 (50).

Our results also establish that both the TL and SI3 significantly contribute to the formation or lifetime of both the elemental and RNA duplex-containing paused states. When the TL and SI3 were deleted, U19 ECs elongated at a single rate, suggesting that ΔTL ECs do not partition into a paused state distinct from the elongation pathway (Table 2). Even after exit-channel duplex formation, ΔTL ECs continue elongation at essentially the same rate. These findings are consistent with previous reports

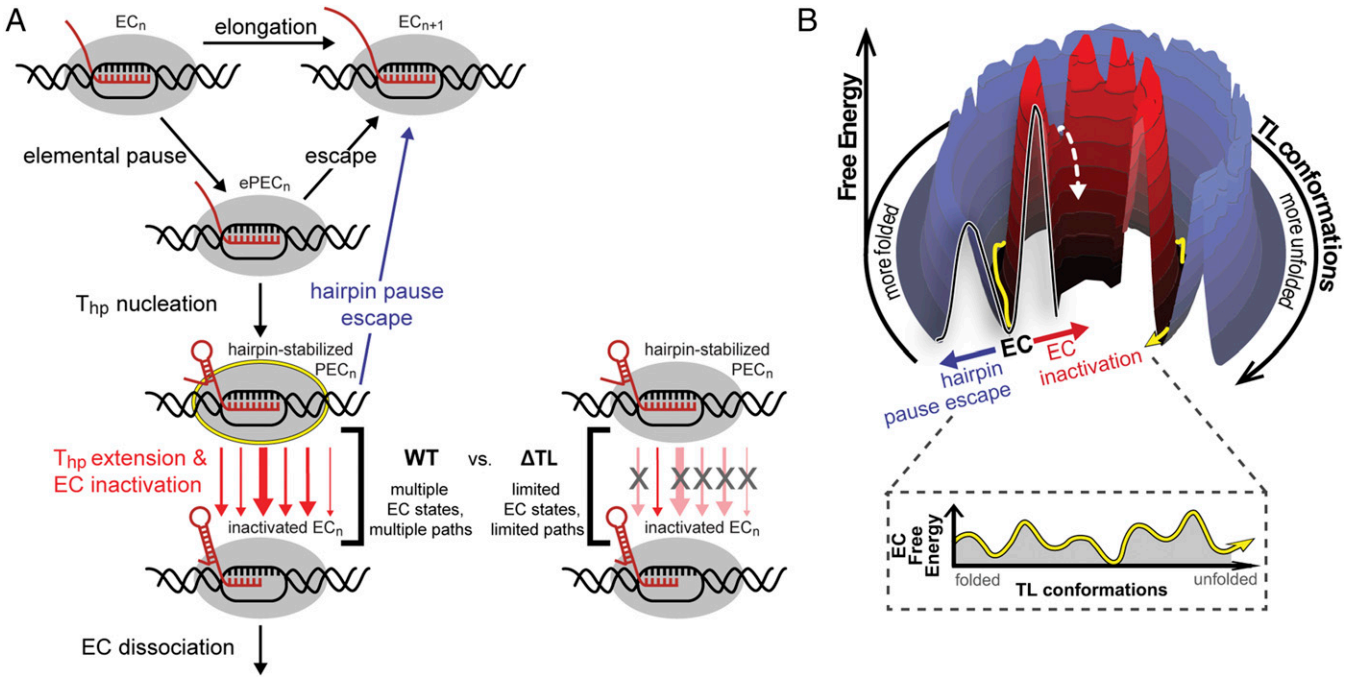

Fig. 6. TL dynamics increase conformational states of an EC and paths to termination. (*A*) The MS-MP model of intrinsic termination. Terminating ECs may exist in a family of conformational states with varying stabilities and access to multiple paths to termination. A WT EC with a dynamic TL occupies a diverse distribution of states, enabling access to many paths of EC inactivation (left). The limited EC dynamics of ΔTL ECs (or ECs with restricted TL flexibility) decrease the number of available paths to EC inactivation (right). Thick arrows indicate paths that are more favorable for termination. (*B*) Hypothetical energy landscape depicting the role of TL conformation in allowing the EC to sample various pathways to termination with differing energy barriers. Blue and red arrows for hairpin pause escape and EC inactivation, respectively, represent the corresponding steps in *A*. The white dashed arrow indicates a hypothetical low-energy barrier that could be more easily traversed by ECs; the yellow arrow denotes the region of the 3D projection analogous to the yellow arrow in *Inset*. (*Inset*) Hypothetical energy diagram depicting the role of TL conformation in altering EC stability.

that the TL significantly contributes to pausing (22), and that altering the TL can decrease both pause efficiency and duration (37, 45).

Of particular interest, we observed that SI3 greatly prolongs the U-tract elemental pause. The presence of SI3 not only increased pause duration ∼15-fold, it also increased the fraction of ECs entering the pause from ∼17 to ∼33% (Table 2). Indeed, the major effect of SI3 on termination is to increase flux toward the termination pathway by increasing pausing, since SI3 had little effect on the rate of termination. Of note, SI3 is surface-exposed, and mAbs that bind SI3 can modulate TL function (28, 48). SI3 may thus present a target for extrinsic regulators that could modulate the flux of ECs into the termination pathway.

Overall, our results suggest that the TL stimulates termination not only by allowing access to lower-energy termination pathways but also, aided by SI3, by increasing entry into and retention of paused EC states that provide time for the T_{hp} to destabilize the EC (Fig. 6).

Conclusion

We suggest that, in addition to NA rearrangements, RNAP dynamics play an important role in intrinsic termination based on the contributions of the TL to multiple decision points in the termination pathway. The TL is a universally conserved polymorphous module in all multisubunit RNAPs (32, 34, 37) whose conformational fluctuations are known to aid steps in the nucleotide addition cycle. Based on our results suggesting a role of TL dynamics in intrinsic termination, we propose an MS-MP model of intrinsic termination that links TL conformational changes to stability of the EC more generally.

Other highly dynamic or mobile domains of RNAP such as the clamp, switch regions, bridge helix, and flap also likely play important roles in both the termination pathway and RNAP dynamics. Our assay provides an easily adaptable method to test their contributions to each step of the termination pathway, and to characterize more completely the structural mechanism by which intrinsic termination disassembles the extraordinarily stable EC.

It is unclear if similar dynamics affect termination by eukaryotic RNAPII, but RNA secondary structures have also been proposed to aid RNAPII termination (63, 64), including effects of bacterial intrinsic terminators in yeast RNAPII (8) and the HIV-1 TAR hairpin on human RNAPII (65). Alterations of the TL in yeast RNAPIII also affect TE (66), and the presence of the TL in archaeal RNAP prevents aberrant termination (67). These findings raise the possibility that the MS-MP termination model may also be relevant to eukaryotic and archaeal RNAPs. Further study of the role of TL dynamics and RNA-structure-mediated termination in eukaryotes and archaea is merited.

Materials and Methods

Sources of materials and proteins are described in *SI Appendix, Supplementary Methods*.

In Vitro EC Reconstitution. The NA scaffold for EC reconstitution was formed by mixing 5 μM G17 RNA and 10 μM T-DNA (template-DNA; #10002 and #8451, respectively; *SI Appendix*, Table S2) in reconstitution buffer (10 mM Tris·HCl, pH 7.9, 40 mM KCl, 5 mM $MgCl_2$), heating to 95 °C for 2 min, cooling rapidly to 45 °C, and then cooling to 25 °C in 2 °C increments for 2 min each, as described previously (68). The 17-nt RNA was designed to have 8 nt of complementarity to the T-DNA at the site of reconstitution to prevent base pairing of upstream T-DNA and RNA, and backtracking of ECs at the termination site.

ECs were reconstituted by incubating 2.5 μM core *E. coli* RNAPs with 0.5 μM NA scaffold in transcription buffer (TB; 20 mM Tris-OAc, pH 8.0, 75 mM NaOAc, 1 mM $Mg(OAc)_2$, 1 mM DTT, 0.1 mM EDTA, 2.5% glycerol, and 25 μg of acetylated BSA/mL) for 15 min at 37 °C. NT-DNA (nontemplate-DNA; #8450; *SI Appendix*, Table S2) was then added at 1.5 μM and incubated for another 15 min at 37 °C. Fully complementary NT-DNA was used to allow

the energy of DNA reannealing upon termination and bubble collapse to contribute to the termination energetics.

In Vitro Transcription. ECs were diluted in TB to 100 nM ECs and radiolabeled by incubation with 0.1 μM [α-^{32}P]CTP and 0.9 μM CTP for 5 min (for WT, ΔSI3, and Ala_6ΔSI3 ECs) or 0.1 μM [α-^{32}P]CTP and 2.5 μM CTP for 30 min (for ΔTL, LTPP, and LTPPΔSI3 ECs) to form C18 ECs. Transcription was restarted by mixing the C18 ECs with an equal volume of TB containing UTP and ATP (to the final concentrations indicated in the reaction schemes of Fig. 3 and *SI Appendix*, Figs. S7, S8, and S10) with or without 50 μM asRNA (100 μM asRNA for Ala_6ΔSI3 ECs). All NTP mixes were supplemented with $Mg(OAc)_2$ at a concentration equivalent to the NTP concentration to avoid Mg^{2+} sequestration effects. Samples incubated for 4 s or longer were stopped manually with an equal volume of 2× stop buffer (10 M urea, 50 mM EDTA, 90 mM Tris-borate buffer, pH 8.0, 0.02% bromophenol blue and 0.02% xylene cyanol). Samples incubated for 8 s or shorter were stopped using a rapid mixing quench flow apparatus (RQF-3; KinTek Corporation) by injecting 100 nM C18 ECs in one sample loop, and UTP and ATP in TB in the presence or absence of 100 μM asRNAs in the other sample loop. Samples obtained at the same times (4 s and 8 s) in the manual and quench flow reactions were similar, verifying that results from the two methods could be merged. Quench flow reactions were stopped with 2 M HCl, and neutralized immediately to pH 7.8 by addition of an equal volume of 3 M Tris base. RNA products were purified by phenol:chloroform extraction followed by ethanol precipitation, and resuspended in 1× stop buffer. RNA products from all timed samples were resolved by 8 M urea denaturing PAGE. Gels were exposed to phosphorimager screens, scanned using the Typhoon PhosphorImager and quantified using ImageQuant software (GE Healthcare).

For dissociation assays (Fig. 2*D*), reconstituted G17 ECs were diluted to 100 nM in TB and tethered to paramagnetic Co^{2+} beads (Dynabeads; Thermo Fisher) through the His_{10} tag on RNAP by incubating with the beads for 10 min at room temperature, followed by 10 min at 37 °C. ECs were radiolabeled by incubation with 0.1 μM [α-^{32}P]CTP and 0.9 μM CTP for 5 min, then beads were washed three times with an equal volume of TB to remove unincorporated CTP and unbound RNAP and NAs. Reactions were restarted by UTP and ATP addition in the presence or absence of 50 μM asRNA. Supernatant samples were taken by magnetic partitioning, and supernatant and whole reaction samples were stopped with an equal volume of 2× stop buffer. RNA products were separated by 8 M urea denaturing PAGE, and visualized by phosphorimaging, as described above.

Kinetic Fitting of Transcription Assay Reaction Progress Plots. Reaction progress curves for C18, U19, and $A20^+$ were generated by calculating the radioactive signal for each RNA species as a percent of total signal from these RNAs in each sample. A20 and all RNAs longer than A20 were combined to give the $A20^+$ fraction.

The reaction progress curves were fit by comparison with numerical integration of kinetic models (e.g., Fig. 4*A*) using KinTek Explorer (KinTek Corporation) (42). All replicates for a given condition and RNAP variant were fit simultaneously (global fitting) to minimize effects of experimental error. Each replicate was also fit individually, and the SDs in the best-fit kinetic parameters were calculated to estimate errors in the rate constants obtained from the global fits.

To determine the elongation kinetics (and pausing kinetics, where applicable) at the termination site in the absence of termination, reactions performed in the absence of asRNA were used. Data were first fit to the simplest model,

$$C18_e \rightarrow U19_e \rightarrow A20^+.$$

The Kintek Explorer fits were seeded with initial rate constants for these two reactions obtained from algebraic, single-exponential fits for C18 disappearance and $A20^+$ appearance using Igor Pro (WaveMetrics). All elongation kinetic models required inclusion of a termination step to fit the data adequately (e.g., Fig. 4*B* and *SI Appendix*, Fig. S3) due to weak termination that occurred at U19 even in the absence of asRNA. If the simple model failed to fit to the data adequately (as evidenced by high residuals with systematic error), pause steps for C18, U19, or both were added to the model to enable a good fit to the data (e.g., Fig. 4*A* and *SI Appendix*, Fig. S10*C*). In these cases, initial rate estimates from double exponential fits of the relevant reactions obtained with Igor Pro were used to seed the Kintek Explorer fits, with the faster rates corresponding to elongation and the slower rates corresponding to pause escape (e.g., $C18_p \rightarrow U19_e$ in Fig. 4*A*). For conditions exhibiting biphasic extension of C18 to U19, reaction kinetics were modeled using two C18 populations with different UMP incorporation rates. For computational simplicity, we fit the two C18 populations using a variable rapid rate to generate the second slow state (e.g., Fig. 4*A*). However, the method of modeling C18 extension kinetics does not impact U19 kinetics (*SI Appendix*, Fig. S12), which were used for all comparisons in this work. We include C18 ECs in the kinetic models only because it is necessary to analyze the kinetic behavior of U19 ECs. We restrict our conclusions about termination to the behavior of the active U19 ECs. Although the halted C18 ECs partitioned into different states with different elongation rates, as shown by Pasman and von Hippel (39), ECs revert to a naïve conformational state after each round of nucleotide addition. Thus, the U19 ECs are expected to be active ECs independent of the rate or path by which they form from C18. Steps with unconstrained rates were added to the kinetic models only if they were justifiable based on known pause or dissociation propensities of the RNAP variants in question, and if the probability that the more complex model gave a better fit was greater than 0.95. The relative probabilities of the selected kinetic models were evaluated against simpler models with fewer unconstrained rates using the corrected Akaike's Information Criterion (AICc) (43),

$$\mathrm{AICc} = N \ln\left(\frac{SS}{N}\right) + 2K + \left(\frac{2K(K+1)}{N-K-1}\right),$$

where n is number of data points, SS is sum of squares, and K is number of free parameters + 1, and

$$\text{probability that selected model is correct}(P) = \frac{e^{-0.5\Delta AICc}}{1+e^{-0.5\Delta AICc}},$$

where ΔAICc is AICc(selected model) − AICc(alternate model) (*SI Appendix*, Figs. S3 and S6).

In conditions with asRNA, elongation and pause kinetics were assumed to be unchanged, since these occur before asRNA binding (e.g., compare Figs. 4*B* and 5*B*), and the relevant rate constants were thus constrained in these fits. Binding and off rates (k_{on} and k_{off}) for asRNA, asRNA concentration, and time of asRNA addition were input into the models and also constrained. Since we observed some amount of terminator escape from C18 and U19, as well as some termination (evidenced by plateaus formed by C18 and U19 with a percent occupancy of >0%; Fig. 5), four steps were added to these conditions: termination at C18, termination at U19, elongation of asRNA-bound C18, and elongation of asRNA-bound U19 (e.g., black arrows in Fig. 5*B*). The only free parameters in these fits were thus the rate constants for these four reactions, obtained by fitting the relevant kinetic models to their datasets by global and individual fitting (see also *SI Appendix*, Fig. S6).

ACKNOWLEDGMENTS. We thank members of the Landick group and Daniel Roston for helpful discussion and comments on the manuscript. This work was funded by the US National Institutes of Health (Grant GM038660 to R.L.). A.R.S. was partially supported by a fellowship from the Department of Biochemistry, University of Wisconsin–Madison.

1. Peters JM, et al. (2012) Rho and NusG suppress pervasive antisense transcription in *Escherichia coli*. *Genes Dev* 26:2621–2633.
2. Arndt KM, Chamberlin MJ (1988) Transcription termination in *Escherichia coli*. Measurement of the rate of enzyme release from Rho-independent terminators. *J Mol Biol* 202:271–285.
3. Helmrich A, Ballarino M, Nudler E, Tora L (2013) Transcription-replication encounters, consequences and genomic instability. *Nat Struct Mol Biol* 20:412–418.
4. Wilson KS, von Hippel PH (1994) Stability of *Escherichia coli* transcription complexes near an intrinsic terminator. *J Mol Biol* 244:36–51.
5. Yager TD, von Hippel PH (1991) A thermodynamic analysis of RNA transcript elongation and termination in *Escherichia coli*. *Biochemistry* 30:1097–1118.
6. Wilson KS, von Hippel PH (1995) Transcription termination at intrinsic terminators: The role of the RNA hairpin. *Proc Natl Acad Sci USA* 92:8793–8797.
7. Greive SJ, von Hippel PH (2005) Thinking quantitatively about transcriptional regulation. *Nat Rev Mol Cell Biol* 6:221–232.
8. Komissarova N, Becker J, Solter S, Kireeva M, Kashlev M (2002) Shortening of RNA: DNA hybrid in the elongation complex of RNA polymerase is a prerequisite for transcription termination. *Mol Cell* 10:1151–1162.
9. Korzheva N, et al. (2000) A structural model of transcription elongation. *Science* 289: 619–625.
10. Vassylyev DG, Vassylyeva MN, Perederina A, Tahirov TH, Artsimovitch I (2007) Structural basis for transcription elongation by bacterial RNA polymerase. *Nature* 448: 157–162.
11. Nudler E, Avetissova E, Markovtsov V, Goldfarb A (1996) Transcription processivity: Protein-DNA interactions holding together the elongation complex. *Science* 273: 211–217.

12. Wilson KS, Conant CR, von Hippel PH (1999) Determinants of the stability of transcription elongation complexes: Interactions of the nascent RNA with the DNA template and the RNA polymerase. *J Mol Biol* 289:1179–1194.
13. Korzheva N, Mustaev A, Nudler E, Nikiforov V, Goldfarb A (1998) Mechanistic model of the elongation complex of *Escherichia coli* RNA polymerase. *Cold Spring Harb Symp Quant Biol* 63:337–345.
14. Sidorenkov I, Komissarova N, Kashlev M (1998) Crucial role of the RNA:DNA hybrid in the processivity of transcription. *Mol Cell* 2:55–64.
15. Martin FH, Tinoco I, Jr (1980) DNA-RNA hybrid duplexes containing oligo(dA:rU) sequences are exceptionally unstable and may facilitate termination of transcription. *Nucleic Acids Res* 8:2295–2299.
16. Toulokhonov I, Artsimovitch I, Landick R (2001) Allosteric control of RNA polymerase by a site that contacts nascent RNA hairpins. *Science* 292:730–733.
17. Weixlbaumer A, Leon K, Landick R, Darst SA (2013) Structural basis of transcriptional pausing in bacteria. *Cell* 152:431–441.
18. Gusarov I, Nudler E (1999) The mechanism of intrinsic transcription termination. *Mol Cell* 3:495–504.
19. von Hippel PH, Yager TD (1991) Transcript elongation and termination are competitive kinetic processes. *Proc Natl Acad Sci USA* 88:2307–2311.
20. Yarnell WS, Roberts JW (1999) Mechanism of intrinsic transcription termination and antitermination. *Science* 284:611–615.
21. Larson MH, et al. (2014) A pause sequence enriched at translation start sites drives transcription dynamics in vivo. *Science* 344:1042–1047.
22. Toulokhonov I, Zhang J, Palangat M, Landick R (2007) A central role of the RNA polymerase trigger loop in active-site rearrangement during transcriptional pausing. *Mol Cell* 27:406–419.
23. Lubkowska L, Maharjan AS, Komissarova N (2011) RNA folding in transcription elongation complex: Implication for transcription termination. *J Biol Chem* 286: 31576–31585.
24. Larson MH, Greenleaf WJ, Landick R, Block SM (2008) Applied force reveals mechanistic and energetic details of transcription termination. *Cell* 132:971–982.
25. Peters JM, Vangeloff AD, Landick R (2011) Bacterial transcription terminators: The RNA 3′-end chronicles. *J Mol Biol* 412:793–813.
26. Santangelo TJ, Roberts JW (2004) Forward translocation is the natural pathway of RNA release at an intrinsic terminator. *Mol Cell* 14:117–126.
27. Ray-Soni A, Bellecourt MJ, Landick R (2016) Mechanisms of bacterial transcription termination: All good things must end. *Annu Rev Biochem* 85:319–347.
28. Epshtein V, Cardinale CJ, Ruckenstein AE, Borukhov S, Nudler E (2007) An allosteric path to transcription termination. *Mol Cell* 28:991–1001.
29. Chakraborty A, et al. (2012) Opening and closing of the bacterial RNA polymerase clamp. *Science* 337:591–595.
30. Gnatt AL, Cramer P, Fu J, Bushnell DA, Kornberg RD (2001) Structural basis of transcription: An RNA polymerase II elongation complex at 3.3 A resolution. *Science* 292: 1876–1882.
31. Sekine S, Murayama Y, Svetlov V, Nudler E, Yokoyama S (2015) Ratcheting of RNA polymerase toward structural principles of RNA polymerase operations. *Transcription* 6:56–60.
32. Vassylyev DG, et al. (2007) Structural basis for substrate loading in bacterial RNA polymerase. *Nature* 448:163–168.
33. Vassylyev DG, et al. (2002) Crystal structure of a bacterial RNA polymerase holoenzyme at 2.6 A resolution. *Nature* 417:712–719.
34. Wang D, Bushnell DA, Westover KD, Kaplan CD, Kornberg RD (2006) Structural basis of transcription: Role of the trigger loop in substrate specificity and catalysis. *Cell* 127: 941–954.
35. Kashlev M, Komissarova N (2002) Transcription termination: Primary intermediates and secondary adducts. *J Biol Chem* 277:14501–14508.
36. Zhang J, Palangat M, Landick R (2010) Role of the RNA polymerase trigger loop in catalysis and pausing. *Nat Struct Mol Biol* 17:99–104.
37. Windgassen TA, et al. (2014) Trigger-helix folding pathway and SI3 mediate catalysis and hairpin-stabilized pausing by *Escherichia coli* RNA polymerase. *Nucleic Acids Res* 42:12707–12721.
38. Mejia YX, Nudler E, Bustamante C (2015) Trigger loop folding determines transcription rate of *Escherichia coli*'s RNA polymerase. *Proc Natl Acad Sci USA* 112:743–748.
39. Pasman Z, von Hippel PH (2002) Active *Escherichia coli* transcription elongation complexes are functionally homogeneous. *J Mol Biol* 322:505–519.
40. Artsimovitch I, Landick R (1998) Interaction of a nascent RNA structure with RNA polymerase is required for hairpin-dependent transcriptional pausing but not for transcript release. *Genes Dev* 12:3110–3122.
41. Shankar S, Hatoum A, Roberts JW (2007) A transcription antiterminator constructs a NusA-dependent shield to the emerging transcript. *Mol Cell* 27:914–927.
42. Johnson KA, Simpson ZB, Blom T (2009) Global kinetic explorer: A new computer program for dynamic simulation and fitting of kinetic data. *Anal Biochem* 387:20–29.
43. Motulsky H, Christopoulos A (2004) *Fitting Models to Biological Data Using Linear and Nonlinear Regression: A Practical Guide to Curve Fitting* (Oxford Univ Press, Oxford, UK).
44. Hein PP, et al. (2014) RNA polymerase pausing and nascent-RNA structure formation are linked through clamp-domain movement. *Nat Struct Mol Biol* 21:794–802.
45. Nayak D, Voss M, Windgassen T, Mooney RA, Landick R (2013) Cys-pair reporters detect a constrained trigger loop in a paused RNA polymerase. *Mol Cell* 50:882–893.
46. Lane WJ, Darst SA (2010) Molecular evolution of multisubunit RNA polymerases: Sequence analysis. *J Mol Biol* 395:671–685.
47. Iyer LM, Koonin EV, Aravind L (2004) Evolution of bacterial RNA polymerase: Implications for large-scale bacterial phylogeny, domain accretion, and horizontal gene transfer. *Gene* 335:73–88.
48. Zakharova N, Bass I, Arsenieva E, Nikiforov V, Severinov K (1998) Mutations in and monoclonal antibody binding to evolutionary hypervariable region of *Escherichia coli* RNA polymerase beta′ subunit inhibit transcript cleavage and transcript elongation. *J Biol Chem* 273:24912–24920.
49. Artsimovitch I, Svetlov V, Murakami KS, Landick R (2003) Co-overexpression of *Escherichia coli* RNA polymerase subunits allows isolation and analysis of mutant enzymes lacking lineage-specific sequence insertions. *J Biol Chem* 278:12344–12355.
50. Chan CL, Wang D, Landick R (1997) Multiple interactions stabilize a single paused transcription intermediate in which hairpin to 3′ end spacing distinguishes pause and termination pathways. *J Mol Biol* 268:54–68.
51. Bar-Nahum G, et al. (2005) A ratchet mechanism of transcription elongation and its control. *Cell* 120:183–193.
52. Darst SA, et al. (2002) Conformational flexibility of bacterial RNA polymerase. *Proc Natl Acad Sci USA* 99:4296–4301.
53. Ansari A, et al. (1985) Protein states and proteinquakes. *Proc Natl Acad Sci USA* 82: 5000–5004.
54. Frauenfelder H, Sligar SG, Wolynes PG (1991) The energy landscapes and motions of proteins. *Science* 254:1598–1603.
55. Liu S-Q, Ji X-L, Tao Y, Tan D-Y, Zhang K-Q, Fu Y-X (2012) Protein folding, binding and energy landscape: A synthesis. *Protein Engineering*, ed Kaumaya P (InTech, Rijeka, Croatia), pp 207–252.
56. Henzler-Wildman K, Kern D (2007) Dynamic personalities of proteins. *Nature* 450: 964–972.
57. Reddish MJ, et al. (2014) Direct evidence of catalytic heterogeneity in lactate dehydrogenase by temperature jump infrared spectroscopy. *J Phys Chem B* 118: 10854–10862.
58. Wang H, et al. (2007) Protein dynamics control the kinetics of initial electron transfer in photosynthesis. *Science* 316:747–750.
59. Noé F, Schütte C, Vanden-Eijnden E, Reich L, Weikl TR (2009) Constructing the equilibrium ensemble of folding pathways from short off-equilibrium simulations. *Proc Natl Acad Sci USA* 106:19011–19016.
60. Berlin V, Yanofsky C (1983) Release of transcript and template during transcription termination at the trp operon attenuator. *J Biol Chem* 258:1714–1719.
61. Epshtein V, Dutta D, Wade J, Nudler E (2010) An allosteric mechanism of Rho-dependent transcription termination. *Nature* 463:245–249.
62. Datta K, von Hippel PH (2008) Direct spectroscopic study of reconstituted transcription complexes reveals that intrinsic termination is driven primarily by thermodynamic destabilization of the nucleic acid framework. *J Biol Chem* 283:3537–3549.
63. Zamudio JR, Kelly TJ, Sharp PA (2014) Argonaute-bound small RNAs from promoter-proximal RNA polymerase II. *Cell* 156:920–934.
64. Xie M, et al. (2013) Mammalian 5′-capped microRNA precursors that generate a single microRNA. *Cell* 155:1568–1580.
65. Harwig A, Jongejan A, van Kampen AH, Berkhout B, Das AT (2016) Tat-dependent production of an HIV-1 TAR-encoded miRNA-like small RNA. *Nucleic Acids Res* 44: 4340–4353.
66. Rijal K, Maraia RJ (2016) Active center control of termination by RNA polymerase III and tRNA gene transcription levels in vivo. *PLoS Genet* 12:e1006253.
67. Fouqueau T, Zeller ME, Cheung AC, Cramer P, Thomm M (2013) The RNA polymerase trigger loop functions in all three phases of the transcription cycle. *Nucleic Acids Res* 41:7048–7059.
68. Kyzer S, Ha KS, Landick R, Palangat M (2007) Direct versus limited-step reconstitution reveals key features of an RNA hairpin-stabilized paused transcription complex. *J Biol Chem* 282:19020–19028.